Hindawi
Geofluids
Volume 2022, Article ID 5267143, 17 pages
https://doi.org/10.1155/2022/5267143

Research Article

Study on Blasting Characteristics of Soft-Hard Rock Strata Based on Energy Fields and Particle Expansion Loading Algorithm

Jianbin Cui,[1] Liangfu Xie,[1,2,3] Yongjun Qin,[1,2] Xuejun Liu,[3] Wei Qiao,[1] Zeyu Hu,[1] Liming Wu,[1] Liewang Qiu,[1] and Ke Huang[1]

[1]*College of Civil Engineering and Architecture, Xinjiang University, Urumqi 830017, China*
[2]*Xinjiang Civil Engineering Technology Research Center, Urumqi 830017, China*
[3]*Xinjiang Academy of Architectural Science (Limited Liability Company), Urumqi 83002, China*

Correspondence should be addressed to Liangfu Xie; xieliangfu@xju.edu.cn

Received 30 June 2022; Revised 2 November 2022; Accepted 7 November 2022; Published 21 November 2022

Academic Editor: Xianwei Zhang

Complex geological conditions often make the blasting effect difficult to control. In order to explore the influence of soft-hard rock strata on rock blasting characteristics, based on PFC2D software, combined with particle expansion loading algorithm, the numerical simulation blasting experiments are carried out. Firstly, the rationality of blasting method is verified by single-hole sandstone blasting experiment. Then, the soft-hard composite strata are established, and the single-hole blasting experiments of composite strata, with different distribution thickness of soft rock stratum and hard rock stratum, are carried out. The experimental results are analyzed from three perspectives: crack network state, internal stress of rock mass, and energy field. Results show that (i) the distance between the interface of soft-hard rock and the blasthole seriously affects the blasting effect. The law of crack number varying with the distance is obtained through further analysis. (ii) When detonated in the hard rock, if the structural plane is about 2 times the radius of crushing area from blasthole, the rock mass will be in a relatively high stress state due to the reflection and superposition of stress waves. (iii) When detonated in the hard rock, if the structural plane is about 2 times the radius of crushing area from blasthole, compared with pure hard rock case, the peak kinetic energy and peak friction energy are increased by about 15 times and 2.6 times, respectively, and the peak strain energy is attenuated by 18%.

1. Introduction

The shock wave generated by explosion attenuates with the increase of propagation distance. At a certain distance from the explosion center, the shock wave in rock mass is transformed into continuous stress wave. Structural plane is a geological interface with a certain extension direction and relatively small thickness formed in rock mass. There are many structural planes in natural rock mass, such as joints, fissures, fault fracture zones, and weak intercalations as well as layered rock mass [1–8], which seriously hinder the propagation of stress waves and make it difficult to control the blasting effect. Scholars from home and abroad had conducted in-depth research on the influence of structural plane on rock mass blasting stress wave. Natural rock mass with joints is quite common. The position [9], number [3], angle, and spacing of joints [10] seriously affected the propagation of stress wave. In addition to the joints in the rock, the trend and position of the fault, detonation sequence, and mining depth also seriously affected the propagation law of stress wave [11–13]. Feng et al. [14] discussed the influence of interacting faults on stress propagation induced by explosion load and found that the propagation of stress wave amplified the stress energy through the region between the two faults. Through numerical analysis and simulation experiments, Gao et al. and Gao et al. [15, 16] studied the damage and failure characteristics of coal and rock in the reverse fault caused by blasting stress wave and found that the reflection of blasting stress wave to the reverse fault exacerbated the damage of coal and rock. Weak interlayer is the weak part of rock mass, which often has adverse effects on the project. Wang et al. [17] established the propagation model of stress

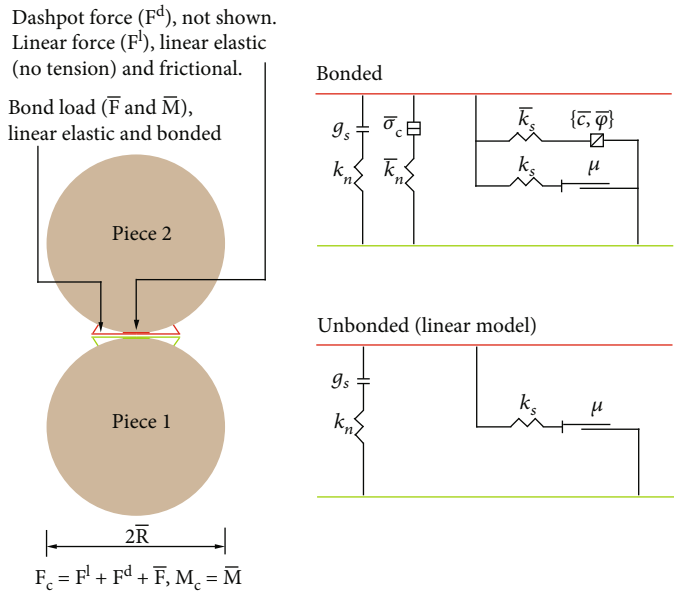

Figure 1: Mechanical behavior of parallel bond model [31].

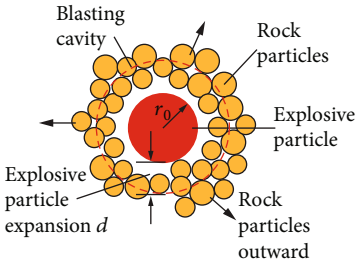

Figure 2: Schematic diagram of blasting load applied by particle expansion [6].

wave in one-dimensional rock mass with weak interlayer, studied the waveform variation law of stress wave, and put forward the dynamic test method of elastic modulus of weak interlayer. Liu et al. [18] believed that the energy of stress wave after the fourth refraction and reflection can be ignored in the process of reciprocating reflection of stress wave in the interlayer. By using numerical simulation method, Sun et al. [19] discussed the influence of the thickness, position, and angle of weak interlayer on the propagation of explosion stress wave.

Soft-hard composite rock strata are often encountered in practical projects such as tunnel excavation and deep resource mining [20–24]. Due to the needs of the project, blasting will be carried out in different positions of the stratum or different strata, and the existence of soft-hard strata makes it difficult to artificially control the blasting quality and effect. In order to make up for the shortcomings of the above scholars in the research of soft-hard rock blasting and make the blasting effect more controllable, this paper establishes the rock mass-blasting numerical model of soft-hard rock and analyzes the blasting characteristics from multiple angles. The conclusions can provide reference for the practical blasting engineering.

2. Basic Principles of PFC2D Method

Geotechnical engineering problems are usually complex. The finite element method (FEM) and finite difference method (FDM) in numerical simulation methods are difficult to solve the large deformation and failure of geotechnical materials. In recent years, the discrete element method (DEM) has been widely used and developed in geotechnical engineering [25–27]. The DEM can solve the mechanical phenomena of complex rock and soil mass that are difficult to explain in geotechnical theory and reveal the failure mechanism and damage deformation of rock and soil mass materials from the macrolevel, mesolevel, and microlevel perspectives. In 1979, Cundall and Strack [28] developed the first two-dimensional discrete element program to simulate the mechanical behavior of granular media. Potyondy and Cundall [29] believe that rock mass materials can be composed of two elements: particles and contacts between particles, in which particles and contacts can be deformed and destroyed. Cho et al. [30] established a numerical model of uniaxial compression test using PFC based on laboratory uniaxial compression test, so as to obtain the microparameters of rock mass.

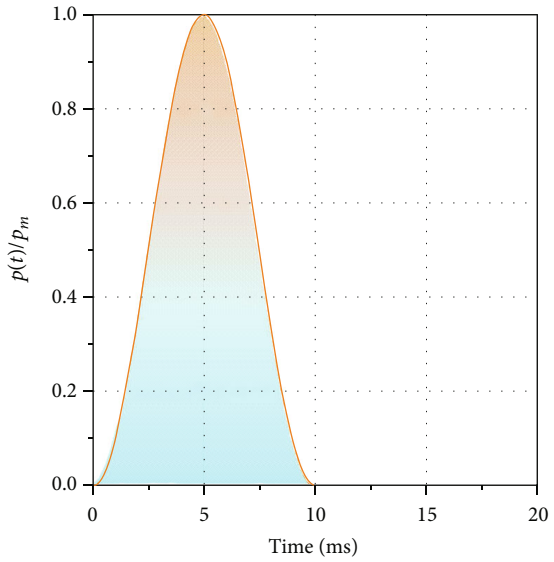

Figure 3: Blasting load loading curve.

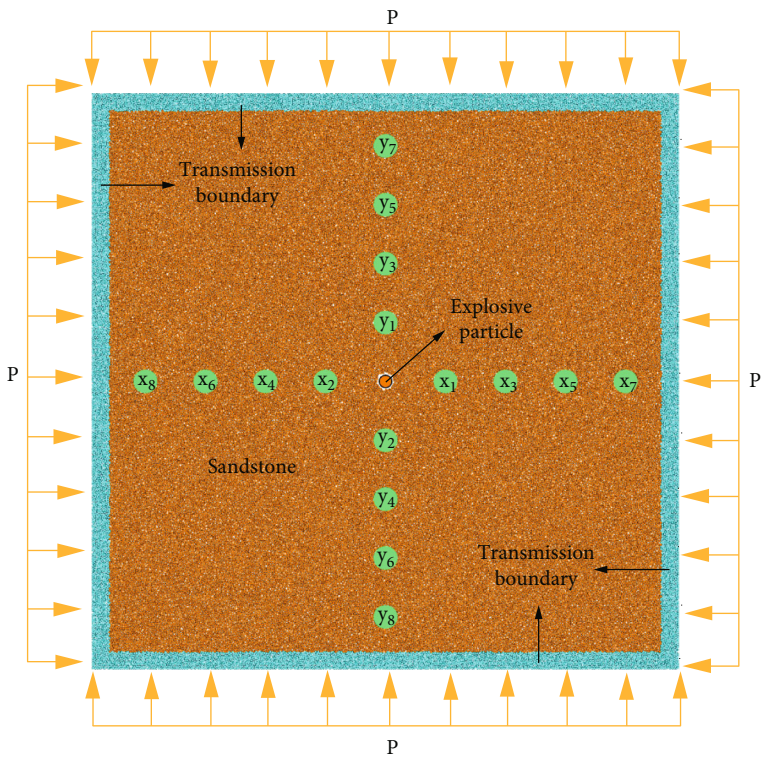

Figure 4: Schematic diagram of single-hole blasting model.

The basic assumptions of the PFC2D method are as follows [6]:

(1) One of the elements of the numerical model, a circular particle, is considered as a rigid body in the program

(2) The contact between particles only occurs in a small area, which can be approximated as point contact

(3) The contact between particles is also one of the elements of the numerical model, and the contact is flexible. And the two particles in the connected state are allowed to have a certain amount of overlap, but the amount of overlap is far less than the radius of the two particles

(4) The contact force and the overlap between particles are connected by the force displacement equation

(5) The contact between particles can establish bonding contact

Table 1: Microscopic parameters of sandstone [31].

Linear group	Parallel-bond group
Effective modulus = 51.0 GPa	Bond effective modulus = 42.0 GPa
Friction coefficient = 1.0	Bond stiffness ratio = 1.0
	Bond tensile strength = 30.0 MPa
Stiffness ratio = 1.0	Bond cohesion = 350.0 MPa
	Bond friction = 65°

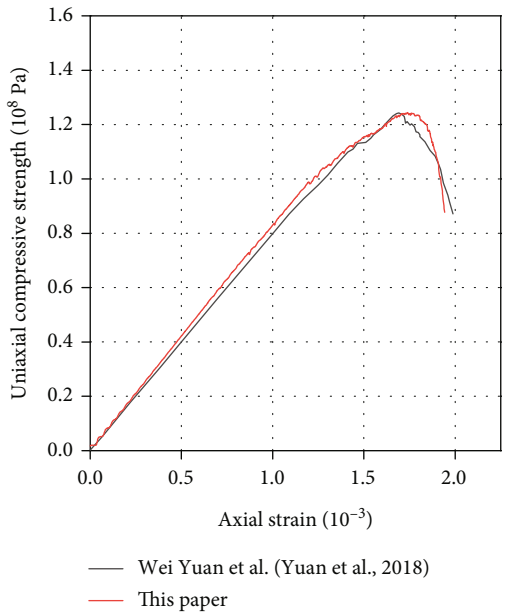

Figure 5: Comparison of uniaxial compression test results of sandstone [35].

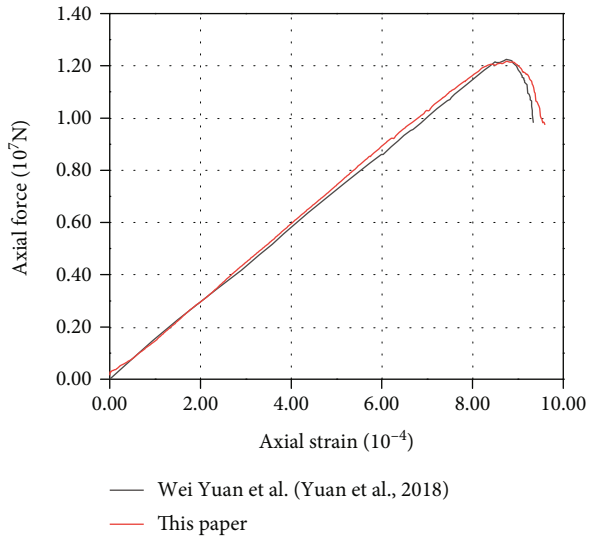

Figure 6: Comparison of Brazilian splitting test results of sandstone [35].

2.1. Basic Control Equations of PFC2D. The PFC2D numerical model is based on the discontinuous medium theory. Because the elements of the medium are discrete particles,

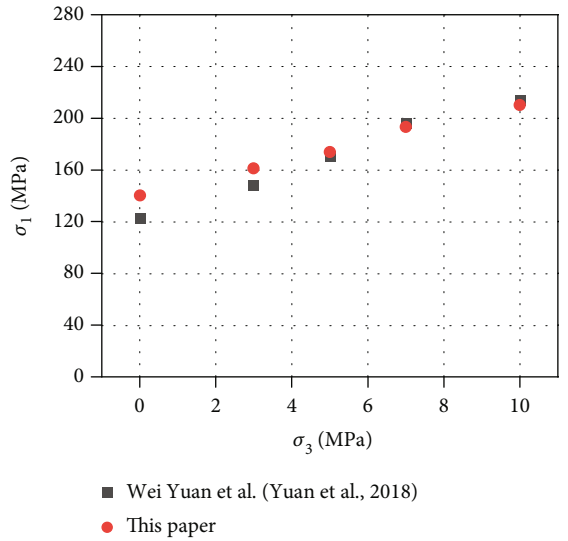

Figure 7: Comparison of biaxial compression test of sandstone [35].

the particle motion is not constrained by the deformation equation. The particle displacement and the contact force between particles are controlled by physical equations. The linear and nonlinear laws in the program change with the particle distribution and stress state. Therefore, the particles only need to satisfy the equilibrium equation. The whole numerical simulation process is based on the force displacement law and Newton's second law. The law of force displacement is reflected in the contact force between particles, and Newton's second law is reflected in controlling the position of particles and readjusting the contact relationship of each element. With the continuous iteration of timestep, the contact force, element position, and contact relationship are updated continuously.

The motion equation of PFC2D is expressed by two sets of vector equations. For translational motion, the equation can be expressed as

$$F = m \cdot (\ddot{x}\text{-}g), \tag{1}$$

where F is the resultant force or the sum of all externally applied forces acting on the particle, $\ddot{x}$ is the acceleration of the particle, m is the mass of the particle, and g is the body force acceleration vector (e.g., gravitational loading).

For rotational motion, the equation can be expressed as

$$L = I\omega, \tag{2}$$

where L is the angular momentum, I is the inertia tensor, and ω is the angular velocity.

2.2. Rock Mass Material Simulation Method. In the numerical simulation experiment of this paper, two contact models in PFC2D are applied, namely, linear model and parallel bond model (Figure 1). Linear model mainly exists in the contact between particles and the wall when the model is established and the contact between particles after material damage. The linear model can be assumed to be a pair of

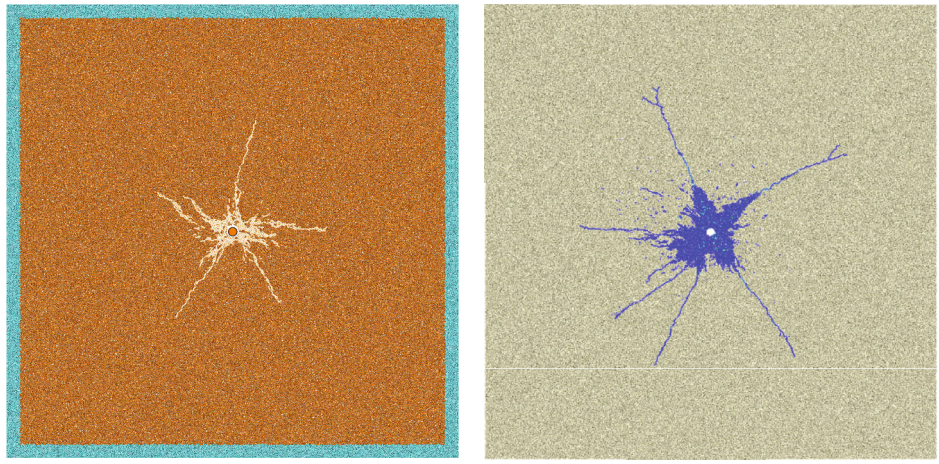

(a) (b)

Figure 8: Numerical simulation (a) [35] in this paper and numerical simulation (b) [31] by Yuan et al.

Table 2: Microscopic parameters of limestone [36].

Linear group	Parallel-bond group
Effective modulus = 2.5 GPa	Bond effective modulus = 2.5 GPa
Friction coefficient = 0.2	Bond stiffness ratio = 1.8
	Bond tensile strength = 10.0 MPa
Stiffness ratio = 1.8	Bond cohesion = 5.0 MPa
	Bond friction = 10°

springs with constant normal stiffness and tangential stiffness, which can transfer normal force and tangential friction, but not moment. Based on linear model, the parallel bond model adds the function of transmitting moment. It mainly exists in the contact between particles when the model is established. The parallel bond model between particles will become a linear model after the material is damaged. The failure conditions are shown in Formula (3) [31].

$$\begin{cases} \sigma_{t\ \max} = \dfrac{\overline{F_n}}{A} + \dfrac{|\bar{M}|}{I}\bar{R}, \\ \tau_{\max} = \dfrac{\overline{F_S}}{A}, \end{cases} \tag{3}$$

where $\sigma_{t\ \max}$ and $\tau_{\max}$ represent the maximum normal stress and the maximum shear stress, respectively. $\overline{F_n}$ and $\overline{F_S}$ represent the normal and tangential component of the parallel-bonded force ($\bar{F}$), respectively. A and I are the area and inertial moment of the bond cross section, respectively. $\bar{R}$ is the bond radius. If the tension stress exceeds the tension strength ($\sigma > \sigma_{t\ \max}$) or the shear stress exceeds the shear strength ($\tau > \tau_{\max}$), it means that the bonded connect is failure, and the corresponding tension crack or shear crack is generated.

2.3. Application of the Explosion Load Based on the Particle Expansion Algorithm. In the numerical simulation of blasting, there are generally three methods to apply blasting load. First, the blasting force is directly applied to the innermost particles of the rock which close to the blasting point. Second, the blasting point compresses the surrounding rock mass through its own expansion to apply blasting stress wave. Third, the velocity of particles around the blasthole is preset and then directly applied to the particles. In this paper, the second blasting point expansion method is selected to apply blasting load [32]. As shown in Figure 2, when the explosion point particle expanded, it will overlap with the particles of the surrounding rock mass.

According to the particle contact principle of PFC2D, the radial force F on the surrounding rock particles after explosion point expansion is

$$F = K_{\mathrm{n}} d = 2\pi r_0 p. \tag{4}$$

Then the explosion point particle expansion radius is

$$d = \frac{2\pi r_0 p}{K_{\mathrm{n}}}, \tag{5}$$

$$K_{\mathrm{n}} = \frac{2(r_{\max} + r_{\min})\pi p}{(r_{\max} - r_{\min})}, \tag{6}$$

where K_{n} is the contact stiffness of particles; r_0 is the initial radius of the blast point; d is the blast point radius after expansion; p is the stress acting on the blasthole wall; $r_{\max}$ and $r_{\min}$ are the maximum radius and minimum radius of the particle expansion, respectively.

The explosion load propagates to the surrounding rock mass with the explosion point as the center, and the action form is equivalent to pulse wave. It is simplified as a half sine wave (as shown in Figure 3) with the same time in the rising section and the falling section, and its expression is

$$p(t) = \frac{p_m}{2}\left(1 - \cos\left(\frac{2\pi}{\Delta T}t\right)\right), \tag{7}$$

where $p(t)$ is the explosion load, p_m is the peak pressure which is 4 GPa, $\triangle T$ is the half sinusoidal action time, generally 10 ms, and t is the duration which is 20 ms.

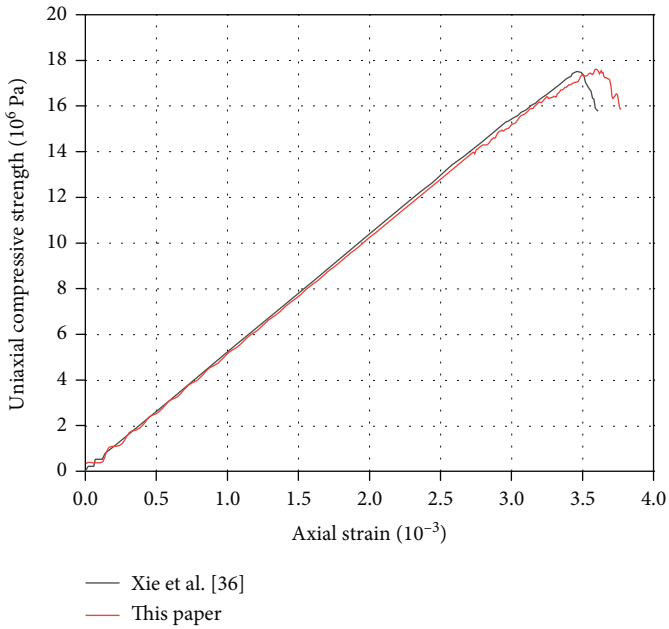

Figure 9: Comparison of uniaxial compression test results of limestone.

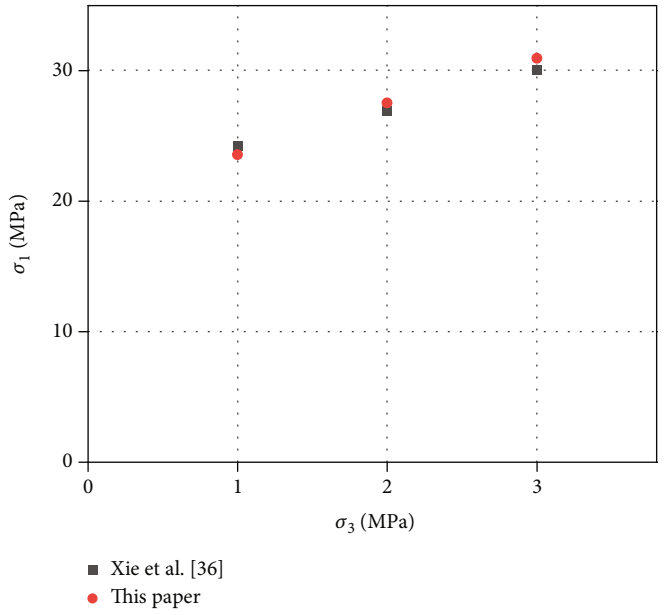

Figure 10: Comparison of biaxial compression test of limestone.

Therefore, the blasting stress wave can be applied to the rock mass as long as the expansion radius of the blasting point is changed according to Equations (7) and (5).

2.4. Configuration of Boundary Conditions. In order to eliminate the reflection of stress wave at the boundary, there are three common methods in numerical simulation [33]. The first method is to expand the model size and dissipate the energy generated by explosion through model internal friction, local damping, and bonding contact, so that the stress wave has been completely dissipated before reaching the boundary. The second method is to fix the velocity and displacement of boundary particles, which is opposite to the effect of stress wave on boundary particles. The third method is to apply boundary force to the boundary particles to meet the requirements of absorbing stress wave energy.

This paper assumes that the rock model is an infinite medium model and ignores the reflection of stress wave at the boundary. Therefore, the method of applying boundary force is adopted, and the stress wave dispersion boundary is set in the PFC2D model to absorb the stress wave propagating to the boundary so that the stress wave does not reflect. This

Table 3: Distribution cases of soft and hard rock stratum.

Case	Height of stratum		Working diagram
	H_S (m)	H_H (m)	
1	0	10	
2	1	9	
3	2	8	
4	3	7	
5	4	6	
6	5	5	
7	6	4	
8	7	3	
9	8	2	
10	9	1	
11	10	0	

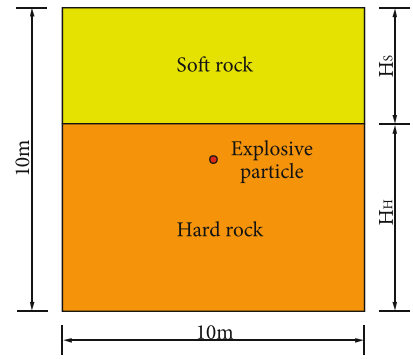

paper considers the viscous boundary proposed by Kouroussis and Verlinden [34] and the dispersion effect of stress wave propagation at rock mass boundary proposed by [32].

The relationship between boundary force and particle moving velocity is

$$F = -2\rho C\dot{u}r, \tag{8}$$

where r is the particle radius, ρ is the rock density, C is the wave velocity, and $\dot{u}$ is the particle velocity.

$$F = \begin{cases} -\xi \cdot 2\rho C_P \dot{u}_n r \\ -\eta \cdot 2\rho C_s \dot{u}_s r \end{cases}, \tag{9}$$

where ζ and η are the dispersion effect correction coefficients of P-wave and S-wave, respectively; C_P and C_S are P-wave velocity and S-wave velocity, respectively; $\dot{u}_n$ and $\dot{u}_s$ are the normal and tangential velocities of particles, respectively.

3. Model Construction and Validation

3.1. Construction of Numerical Single-Hole Blasting Model. The numerical blasting model of single-hole, as shown in Figure 4 is established by using particle flow code (PFC2D). The model size is 10 m × 10 m, a circular explosion point with a radius of 10 cm is set in the geometric center of the model. The model consists of 79372 particles in total. The initial stress field is applied with a compressive pressure P on the four sides of the rock model. Monitoring points, as shown in Figure 4, are established inside the model to monitor the internal stress (x_1~x_8 are the monitoring points in the horizontal direction; y_1~y_8 are the monitoring points in the vertical direction).

Sandstone (hard rock) is taken as the research object to carry out the numerical simulation of single-hole blasting. Yuan et al. carried out the indoor tests and single-hole blasting numerical simulation of sandstone, and the test results were good. Therefore, the microscopic parameters of sandstone obtained by Yuan et al. are used in this paper, as shown in Table 1.

In order to verify the rationality of sandstone microscopic parameters in Table 1, uniaxial compression test, Brazilian splitting test, and biaxial compression test are also carried out in this paper. The experimental comparison results are shown in Figures 5–7, which show that the parameters in Table 1 are accurate and reasonable. What is more, the results of the three tests are identical to those in the literature [35] which is obtained by Cui et al.

3.2. Comparison and Verification of Blasting Results. In the particle flow code (PFC2D), the particle expansion method is used to generate particles with an initial radius range of 5~7.5 mm, and then the servo mechanism proposed by Cundall and Strack [28] is used to set an initial stress field of 5 MPa for the rock sample. When the confining pressure of the sample reaches the target confining pressure, delete the wall and exit the servo. The parallel bond model is selected for the rock sample with the initial stress field, and the microparameters are given to the contact between particles. Finally, set the transmission boundary and apply the blasting load to the blasting point. The whole blasting process lasts for 20 ms, and the final blasting effect is shown in Figure 8(a) which is the same result gained by authors shown in the literature [35]. Under the same model size, rock mechanical properties and initial stress field, the result is basically consistent with that obtained by Yuan et al. [31] (Figure 8(b)), which proves the rationality of the blasting method adopted in this paper.

4. Working Cases Setting

In practical blasting engineering, the condition of multiple strata is quite common. Due to engineering needs, blasting will be carried out at different positions in the same stratum or different strata, which has an important impact on the blasting effect. Based on this, this paper carries out single-hole blasting experiments in soft-hard rock strata.

The confining pressure is the same as that of the single-hole blasting model, which is 5 MPa. And soft rock stratum is introduced to sandstone and study the influence of different soft and hard rock thickness on the blasting effect. Liangfu et al. [36] used PFC2D to conduct uniaxial compression test and biaxial compression test, which accurately calibrated the microparameters of limestone. Thus, this paper takes the group of microparameters of limestone (Table 2) as the parameters of soft rock. Uniaxial compression test and biaxial compression test are also carried out which results are shown in Figures 9 and 10, which prove the accuracy of the parameters in Table 2. The specific distribution cases of soft rock stratum thickness (H_S) and hard rock stratum thickness (H_H) in rock mass model are shown in Table 3.

5. Blasting Results

5.1. Crack Network Analysis. In the process of stress wave propagation, reflection and transmission will occur when encountering faults or joints. When there is little difference between the wave impedance of fillers in faults and media around the blasthole, the energy of stress wave is mainly transmission. On the contrary, the stress wave energy is mainly reflected. The incident compression wave interacts with the reflected tensile wave and other tensile waves to form a stress wave superposition area on the wave front [37]. In addition to the reflection of the structural plane of the rock mass itself, the crack generated in the rock mass during blasting also blocks the reflected stress wave. Therefore, the stress wave will converge on the side of the wave face, which will aggravate the failure of this part of rock mass. It is illustrated in Figure 11 that the corresponding blasting crack network states of structural planes at different positions (11 working cases in Table 3). It can be seen from Figure 11 that the position of structural plane has an important impact on the damage degree of rock.

It can be seen from Figure 11 that the position of structural plane has an important impact on the number and shape of cracks. According to the results of the crack network, the cracks are mainly distributed around the blasthole, and the number of cracks can reflect the damage degree of the rock mass to a certain extent. The more the number of cracks, the higher the degree of rock damage, and vice versa. Therefore, this paper studies the relationship between the thickness of soft rock stratum (H_S) and the total number of cracks under corresponding working cases (Figure 12). As shown in Figure 12, the curve can be divided into three parts:

(1) *The Structural Plane Is above the Blasthole*. As shown in Figure 12, $H_S = 0 \sim 4$ m in the curve (corresponding to working cases 1~5 which are Figures 11(a)–11(e)), explosive is detonated in hard rock, and the stress wave is incident from the hard rock to the soft rock. According to Figure 11, under above working cases, the distance between structural plane and blasthole seriously affects the damage degree of the rock mass. The closer the structural plane is to the blasthole, the more cracks occur in the rock mass, and the longer the length of the main crack. The reason for these phenomena is that the closer the structural plane is to the blasthole, the more the reflected and transmitted stress wave energy is. In addition, the continuous development of cracks also has a barrier effect on the stress wave, resulting in an increase in the stress wave energy that converges between the blasthole and the structural plane, thereby increasing the degree of damage to this part of the hard rock. Similarly, the more the energy of the transmitted stress wave transmitted to the soft rock, the greater the damage degree of the soft rock. Through the simulation of the results obtained from the numerical experiment, the relationship between H_S and the total number of cracks under corresponding working cases can be obtained

$$y = y_0 + \mathrm{A}e^{(-x/\mathrm{B})}, \tag{10}$$

where $y_0 = 1387.29$, $A = 31.34$, and $B = -0.92$.

(2) *The Structural Plane Is near the Blasthole*. As shown in Figure 12, $H_S = 4 \sim 6$ m in the curve (corresponding to working cases 5~7 which are Figures 11(e)–11(g)). When the structural plane changes within 2 times the radius of the crushing area, the number of cracks decreases sharply with the growth of H_S. The main reason for this phenomenon is that the structural plane changes in the shock wave propagation area, so the change trend of rock mass damage degree is quite different from that in the stress wave propagation area. The result can also be fitted to obtain the relationship between the total number of cracks and H_S

$$y = Cx^{\mathrm{D}}, \tag{11}$$

where $C = 121599.21$ and $D = -2.51$.

(3) *The Structural Plane Is below the Blasthole*. As shown in Figure 12, $H_S = 6 \sim 10$ m in the curve (corresponding to working cases 7~11 which are Figures 11(g)–11(k)), the explosive is detonated in soft rock, and the stress wave is incident from soft rock to hard rock. It can be seen from Figure 11 that with the growth of H_S, the numbers of cracks are basically stable at about 1500, and the states of cracks are basically unchanged. The reason for this phenomenon is that the stress wave energy will decrease rapidly in soft rock, so the stress wave reflected and transmitted by the structural plane is quite few, which is not enough to aggravate the damage of rock. This is also the reason why the damage degree of rock mass around the borehole is higher than that detonated in hard rock when detonated in soft rock. It shows that when the explosive is detonated in soft rock, the distance between structural plane and

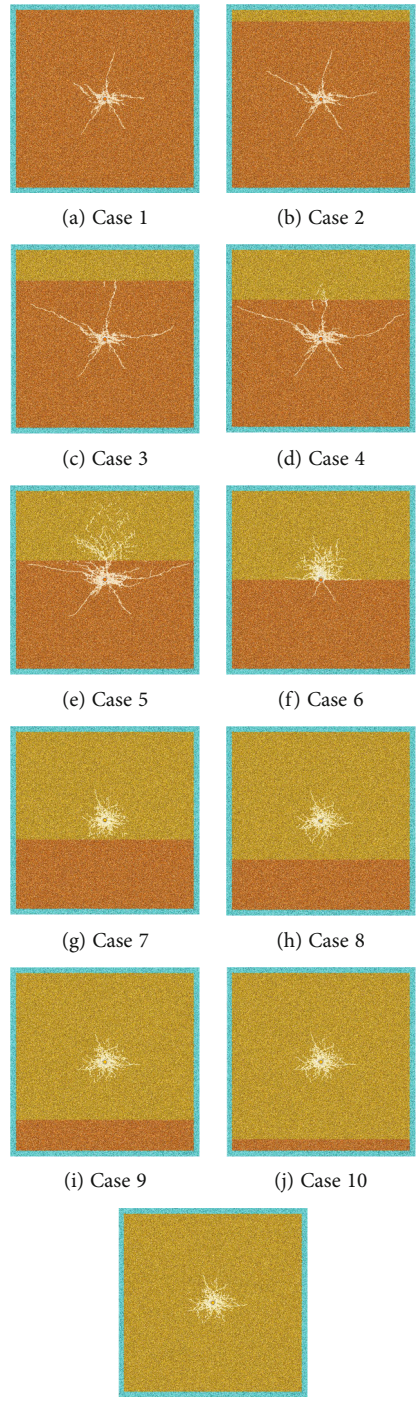

(a) Case 1 (b) Case 2

(c) Case 3 (d) Case 4

(e) Case 5 (f) Case 6

(g) Case 7 (h) Case 8

(i) Case 9 (j) Case 10

(k) Case 11

Figure 11: Blasting effect drawing under different working cases.

blasthole has little effect on the damage degree of rock mass

To sum up, when the structural plane is above the blasthole, the number of cracks increases exponentially with the growth of H_S. When the structural plane is around the blasthole, the number of cracks will decrease sharply with the growth of H_S. When the structural plane is below the blasthole, the state and number of cracks are less affected by the change of H_S.

According to the analysis of Figures 11 and 12:

(1) *Comparing* Figure 11(a)*with* Figure 11(k). Under the working cases of initiation in pure hard rock and pure soft rock, respectively, the total number of cracks is almost the same, but the states of cracks

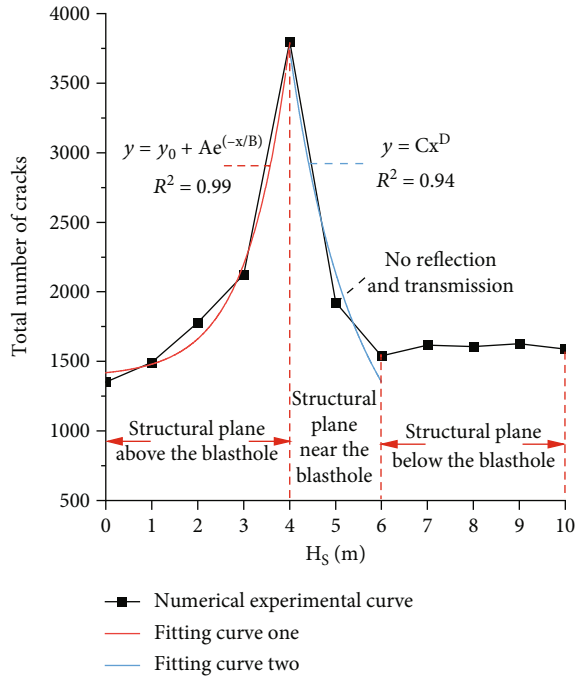

Figure 12: Relationship between H_S and total crack number under corresponding working cases.

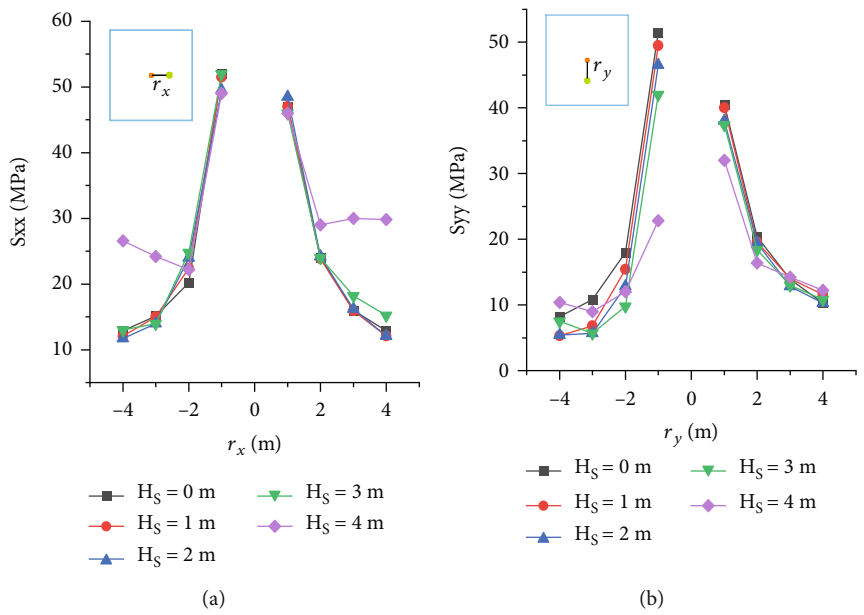

Figure 13: Variation curve of peak stress with r_x and r_y.

are quite different. When initiation in pure hard rock, the crushing area is small, the attenuation of explosion stress wave is slow, and the cracking area is large. Initiation in pure soft rock is opposite to that in pure hard rock, and the crushing area is large, indicating that the stress wave attenuates rapidly in soft rock, resulting in a small range of cracking area. Compared two cases with Figure 11(f), when initiation in the structural plane, it inhibits the development of cracks in hard rock, promotes the development of cracks in soft rock, and the cracks are prone to develop along the structural plane

(2) *Comparing* Figure 11(e)*with* Figure 11(g). When the distance between blasthole and structural plane is the same, the attenuation of stress wave is slow due to

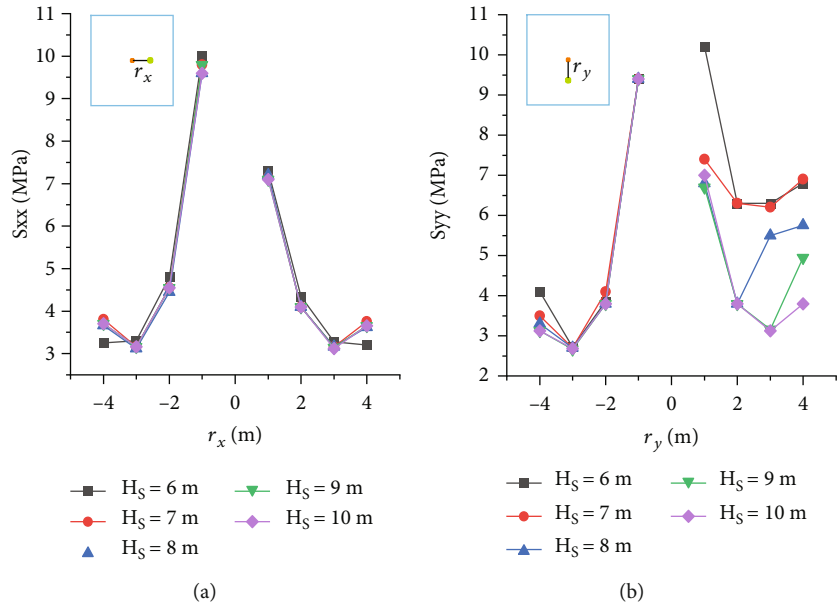

Figure 14: Variation curve of peak stress with r_x and r_y.

the high strength of hard rock, so the stress wave will cause cracking after transmitted to soft rock. In contrast, due to the low strength of soft rock, the stress wave attenuates rapidly, so the stress wave will not cause cracking after transmitted to hard rock

5.2. Internal Stress Analysis of Rock Mass

5.2.1. Initiation in Hard Rock. By using monitoring points x_1 ~x_8 and y_1~y_8, the peak stress Sxx which is parallel to the blasthole direction and the peak stress Syy which is perpendicular to the blasthole direction in working cases 1~5 are set. And the variation curves of the peak stress in the two directions are obtained (Figure 13).

As shown in Figure 13(a), when $H_S = 0$, 1, and 2 m, Sxx decreases rapidly with the increase of r_x. The farther the structural plane is from the blasthole, the less the reflected stress wave is. What is more, there is the blocking effect of the cracks on the stress wave, so the superposition effect of the stress wave parallel to the blasthole is not obvious. When $H_S = 3$ and 4 m, the attenuation trend of Sxx begins to change. Especially when $H_S = 4$ m, the change trend of Sxx tends to decrease and then increase, indicating that when the structural plane is 2 times the radius of crushing area away from the blasthole, the stress wave will be seriously reflected and superimposed on both sides of the blasthole, resulting in high internal stress in the rock mass far away from the blasthole.

As shown in Figure 13(b), the change trend of Syy with H_S is relatively consistent. The impact of H_S on Syy is mainly reflected in that when r_y is 1 m, Syy decreases with the increase of H_S. Especially, when initiation in hard rock, the Syy decreases exponentially. The closer the structural plane is to the blasthole, the more stress wave is reflected. In addition, the blocking effect of the cracks on the stress wave will lead to the higher energy gathered in the rock mass between blasthole and structural plane, and finally the higher the damage degree of the rock mass. Therefore, the higher the attenuation amplitude of the stress wave.

In conclusion, when initiation in hard rock and the structural plane is within 2 times the radius of the crushing area ($H_S = 4$ m), Sxx decreases first and then increases with the growth of r_x, so the hard rock between blasthole and structural plane is in a high stress state. With the increase of H_S, the peak stress Syy perpendicular to the blasthole direction decays rapidly in an exponential.

5.2.2. Initiation in Soft Rock. The variation curves of Sxx and Syy in working cases 7~11 are shown in Figure 14.

As shown in Figure 14(a), the change trend of Sxx is relatively consistent, decreases rapidly with the increase of r_x and is hardly affected by the change of H_S. It shows that the stress wave decays rapidly in soft rock and is consumed a lot before it propagates to the structural plane. Therefore, there are few reflected stress waves, resulting in a small impact of the change of H_S on Sxx.

As shown in Figure 14(b), the change trend of Syy is also relatively consistent, which also shows that the change of H_S has little impact on the Syy in the upper rock mass. However, the change of H_S has a great impact on the Syy in the lower rock mass. With the increase of H_S, the Syy at the place where r_y is 1 m decreases rapidly. Under the same working case of H_S, the Syy shows an increasing trend with the growth of r_y. when $r_y > 2$ m.

In conclusion, when initiation in soft rock, with the increase of H_S, the peak stress Syy decreases rapidly at 2 times the radius of crushing area (r_y is 1 m). When H_S is constant, Syy will increase with the growth of r_y. when $r_y > 2$ m.

5.3. Evolution Processes of Energy Fields. In order to explore the influence of the structural plane position on the internal

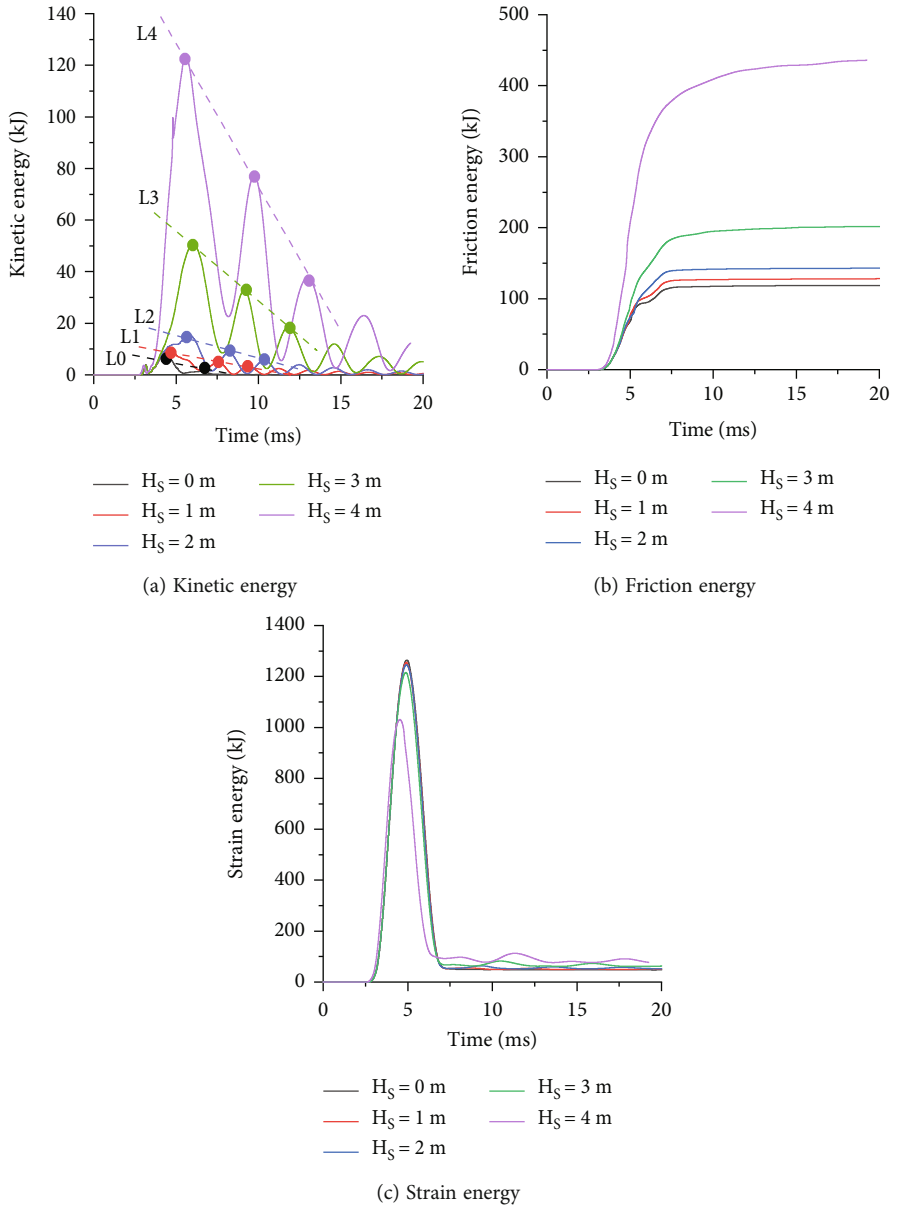

(a) Kinetic energy

(b) Friction energy

(c) Strain energy

Figure 15: Energy evolution curves (1~5 working cases).

energy of rock mass, this paper analyzes the blasting results from the perspective of kinetic energy, friction energy, and strain energy. Three energy calculation methods (Formulas (12)–(14)) are given in the particle flow program (PFC2D). Through the energy records in the software, the energy evolution curves of rock mass can be obtained.

Kinetic energy (E_K) calculation method:

$$E_K = \sum_{i=1}^{n} \frac{1}{2} m_i v_i^2, \tag{12}$$

where m_i is the mass of the particle, v_i is the velocity of the particle, and n is the total number of particles.

Friction energy (E_F) calculation method:

$$E_F = -F^{\mathrm{d}} \cdot \left(\dot{\delta}\, t\right), \tag{13}$$

where F^{d} is the dashpot force, $\dot{\delta}$ is the relative translation velocity, and t is the during time.

Strain energy (E_S) calculation method:

$$E_S = \frac{1}{2}\left(\frac{F_n^2}{k_n A} + \frac{\|F_s\|^2}{k_s A} + \frac{M_t^2}{k_s J} + \frac{\|M_b\|^2}{k_n I}\right), \tag{14}$$

where k_n is the normal stiffness, k_s is the shear stiffness, A is the cross-sectional area, I is the moment of inertia of the

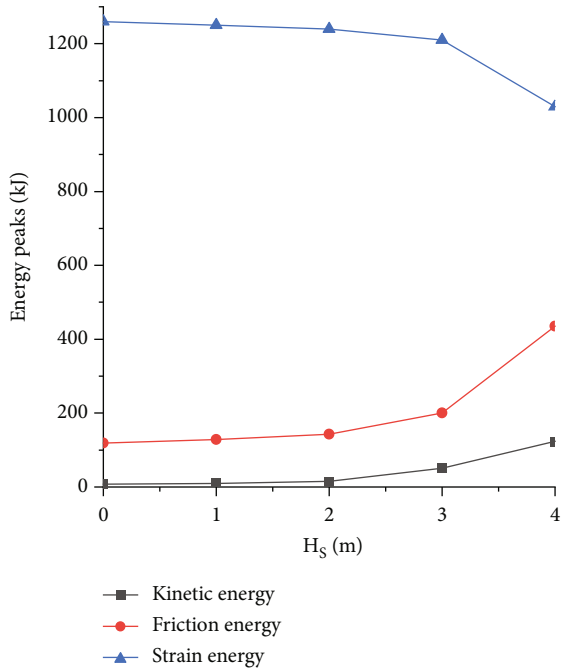

Figure 16: Curves of peak energy versus H_S (1~5 working cases).

parallel bond cross-section, J is the polar moment of inertia of the parallel bond cross-section, F_n is the parallel-bonded normal force, F_s is the parallel-bonded shear force, M_t is the parallel-bonded twisting moment (2D model: $M_t = 0$), and M_b is the parallel-bonded bending moment.

5.3.1. Initiation in Hard Rock. When initiation in hard rock, the evolution processes of kinetic energy, friction energy, and strain energy are shown in Figures 15 and 16.

According to the energy evolution curves, the thickness of soft rock H_S seriously affects the changes of three kinds of energy:

(1) As shown in Figure 15(a), the kinetic energy of the rock mass surges due to the continuous proximity of the structural plane to the blasthole. When initiation in pure hard rock, the peak kinetic energy is 7.7 kJ; when the structural plane is 1 m away from the blasthole, the peak kinetic energy is 124 kJ, which is about 15 times higher than that of pure hard rock

When the blasting duration is about 5 ms, the kinetic energy reaches the first peak value as well as the maximum peak value. As the blasting process proceeds, the kinetic energy amplitude begins to decrease significantly. In order to clearly observe the change of kinetic energy amplitude with the growth of H_S, the inclined lines L0~L4 (representing $H_S = 0 \sim 4$ m) are used to fit the amplitudes. It can be seen that when H_S is constant, the kinetic energy amplitudes decrease linearly. The specific reduction values are shown in Table 4. When there is no structural plane in the rock, the kinetic energy has about two obvious amplitudes, and the second amplitude is about 25% of the first amplitude; when there is a structural plane in the rock, the kinetic energy has at least three obvious amplitudes. Compared with the first amplitude, the second amplitude and the third amplitude are attenuated by about 42% and 65%, respectively.

Table 4: Amplitude attenuation values (1~5 working cases).

Amplitude attenuation	H_S (m)				
	0	1	2	3	4
A_F (%)	75	49	44	36	38
A_S (%)		65	63	64	69

In the table, compared with the first amplitude, the attenuation degrees of the second amplitude and the third amplitude are A_F and A_S, respectively.

(2) As shown in Figure 15(b), as the blasting process proceeds, the friction energy increases rapidly before 7.5 ms and then tends to be stable after 7.5 ms. With the structural plane approaching to the blasthole, the growth degree of friction energy increases rapidly. When initiation in pure hard rock, the peak friction energy is 119 kJ; when the structural plane is 1 m away from the blasthole, the peak friction energy is 435 kJ, which is about 2.6 times higher than that of pure hard rock

(3) As shown in Figure 15(c), as the blasting process proceeds, the strain energy increases rapidly before 5 ms, reaches the peak strain energy at about 5 ms, and decreases sharply at 5~7.5 ms. As the structural plane approaches to the blasthole, the strain energy begins to decay. When initiation in pure hard rock, the peak strain energy is 1260 kJ. When the structural plane is 1 m away from the blasthole, the peak strain energy is 1030 kJ, which is attenuated by 18% compared with pure hard rock

5.3.2. Initiation in Soft Rock. When initiation in soft rock, the evolution processes of kinetic energy, friction energy, and strain energy are shown in Figure 17.

According to the energy evolution curves, the thickness of soft rock H_S has little effect on the three kinds of energy:

(1) As shown in Figure 17(a), the change trend of kinetic energy is similar to the detonation of hard rock. At about 5 ms, the maximum peak value of kinetic energy appears. As the blasting process proceeds, the kinetic energy amplitudes begin to decrease significantly. The inclined lines L6~L10 (representing $H_S = 6 \sim 10$ m) are used to fit the amplitudes. When H_S is constant, the kinetic energy amplitudes also decrease linearly, and the specific reduction values are shown in Table 5. When initiation in soft rock, the kinetic energy curve has at least three obvious amplitudes in every case. Compared with the first amplitude, the second amplitude and the third amplitude are attenuated by about 20% and 56%, respectively

(2) As shown in Figures 17(a)–17(c) and 18, the change trends of kinetic energy, friction energy, and strain energy are the same as that of initiation in hard rock, but the increase of H_S has little impact on three

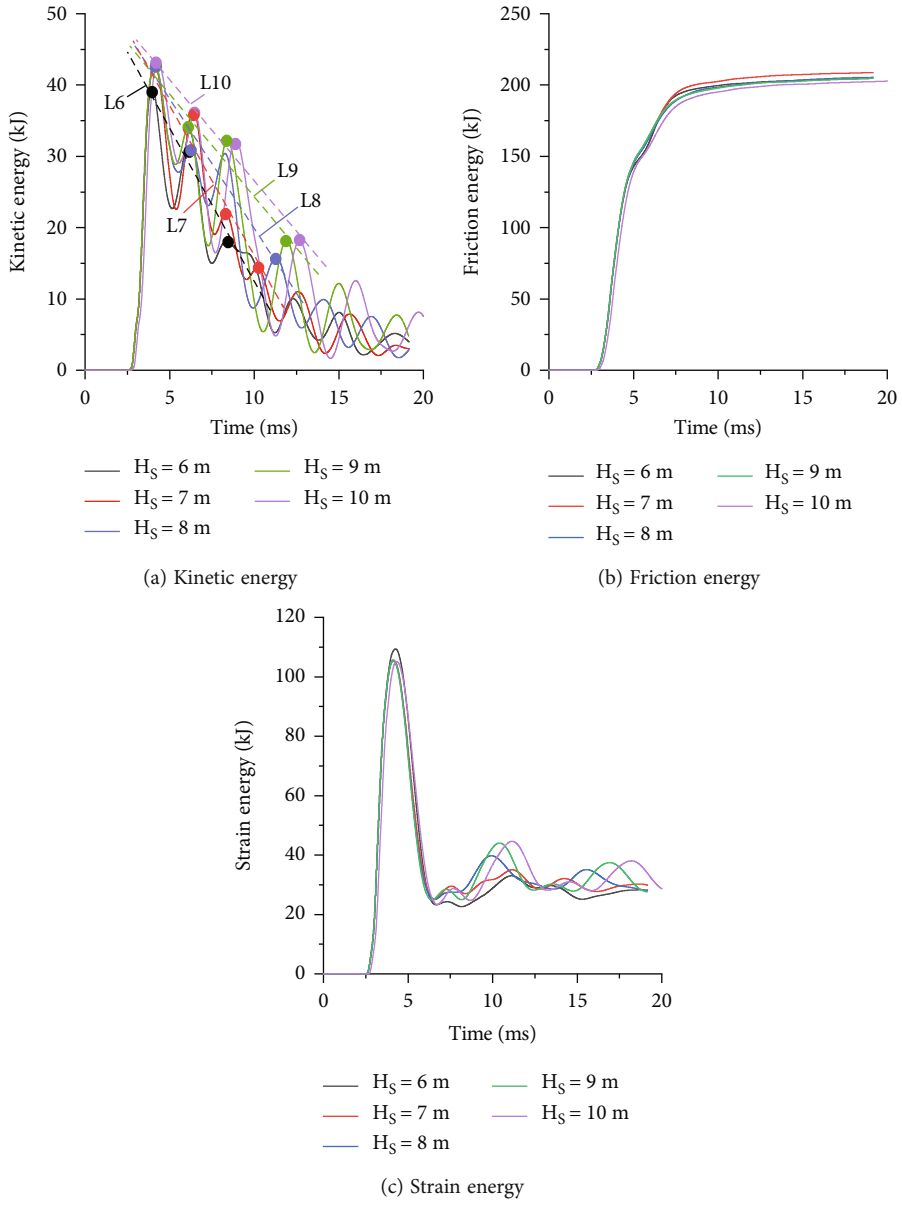

(a) Kinetic energy

(b) Friction energy

(c) Strain energy

Figure 17: Energy evolution curves (7~11 working cases).

Table 5: Amplitude attenuation values (7~11 working cases).

Amplitude attenuation	H_S (m)				
	6	7	8	9	10
A_F (%)	15	17	28	21	26
A_S (%)	54	49	63	58	59

In the table, compared with the first amplitude, the attenuation degrees of the second amplitude and the third amplitude are A_F and A_S, respectively.

energy peaks. The peak kinetic energy, peak friction energy, and peak strain energy are about 43 kJ, 205 kJ, and 105 kJ, respectively

6. Discussions

According to the experiment results obtained from the three angles of crack effect, internal stress of rock mass and energy fields, the detonation position and the distance between blasthole and structural plane seriously affect the blasting characteristics. Therefore, the blasting effect can be more controllable by adjusting the detonation position and the distance between blasthole and structural plane:

(1) The results of detonation in hard rock and soft rock are quite different. Detonation in hard rock can expand the influence range of crack, increase the penetration of cracks, and aggravate the damage of

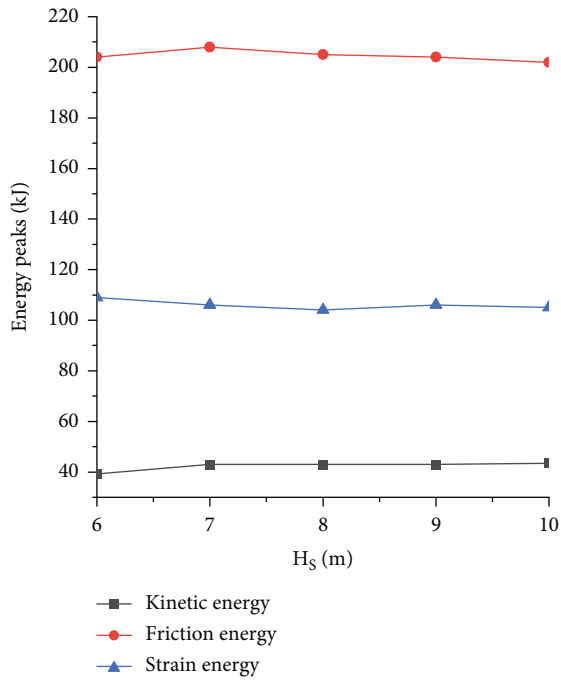

Figure 18: Curves of peak energy versus H_S (7~11 working cases).

rock. It is more suitable for blasting engineering in a large area blasting engineering. When blasting in soft rock, the cracks are relatively concentrated and the influence range of cracks is small, which is more suitable for blasting in a small area blasting engineering. In addition, in the whole process of detonation in hard rock, the rock mass is in a high stress state. When blasting in soft rock, the whole rock mass is in a low stress state, so blasting in soft rock has little impact on the surrounding rock mass

(2) According to the energy field evolution results, when initiation in hard rock and the distance between structural plane and blasthole is less than 2 m, the variation amplitude and energy peak of kinetic energy are large, which will cause large amplitude vibration of the whole rock mass and even the rock mass far away. Although the penetration effect under this working case is good, it also has a great impact on the stability of the surrounding rock mass. When initiation in hard rock and the distance between structural plane and blasthole is more than 2 m, the penetration of cracks in the rock mass is also good, and the peak value of kinetic energy is significantly less than the former which will not cause large-scale vibration of the rock mass far away

(3) In addition to the influence of structural plane position and detonation position on blasting characteristics considered in this paper, due to the complexity of the stratum, there may be many factors such as the existence of joints or resource mining under high temperature and high pressure. These factors will affect the propagation of stress wave and affect the blasting characteristics of rock mass, which make it difficult to accurately control the effect. Based on the complex strata, further in-depth research on these factors will be carried out in the future stage

7. Conclusions

In this paper, the numerical model of rock blasting is established by using particle flow code (PFC2D), and the rationality of hard rock single-hole model blasting method is verified. On this basis, soft rock with different thickness is introduced, and the main conclusions are as follows:

(1) When initiation in hard rock and structural plane is far from the blasthole, crack number increases exponentially with the growth of soft rock thickness. When structural plane is around the blasthole, crack number decreases sharply. When initiation in soft rock, the number and state of cracks are little affected by structural plane position. Based on the first two cases, the variation laws of crack number with soft rock thickness are obtained

(2) When initiation in hard rock and structural plane is about 2 times the radius of crushing area from blasthole, with the increase of the distance between blasthole and horizontal monitoring point, horizontal peak stress Sxx decreases first and then increases. In this case, the rock mass is in a relatively high stress state. With the increase of soft rock thickness H_S, the vertical peak stress Syy decays rapidly in an exponential form at 2 times the radius of crushing area. When initiation in soft rock, with the increase of H_S, Sxx and Syy decrease rapidly and then increase

(3) When initiation in hard rock, the existence of structural plane will increase the kinetic energy in the rock mass, and there are at least three obvious amplitudes in the attenuation process of kinetic energy. Compared with the first amplitude, the second amplitude and the third amplitude are attenuated by 42% and 65%, respectively. When initiation in soft rock, the peak kinetic energy is less affected by structural plane position. There are also at least three obvious amplitudes in the kinetic energy attenuation process. Compared with the first amplitude, the second amplitude and the third amplitude are attenuated by 20% and 56%, respectively

(4) When initiation in hard rock and the structural plane is 2 times the radius of crushing area from blasthole, the three energies change greatly. Compared with pure hard rock case, the peak kinetic energy increases by about 15 times, the peak friction energy increases by about 2.6 times, and the peak strain energy attenuates by about 18%. When initiation in soft rock, the peak values of the three energies are relatively stable and are less affected by the change of structural plane

Data Availability

Some previously reported data were used to support this study and are available at [doi:10.1038/s41598-022-17028-y]. The prior study is cited at the relevant place within the text as the reference [35]. And other data used to support the findings of present study are included in the submitted article.

Conflicts of Interest

The authors declare that they have no competing interests.

Acknowledgments

This project was supported by the National Natural Science Foundation of China (52068066 and 51908482) and the Autonomous Region Graduate Innovation Project (XJ2022G050).

References

[1] H. Liu, B. Zhang, X. Li et al., "Research on roof damage mechanism and control technology of gob-side entry retaining under close distance gob," *Engineering Failure Analysis*, vol. 138, article 106331, 2022.

[2] S. Liu, X. Li, D. Wang, and D. Zhang, "Investigations on the mechanism of the microstructural evolution of different coal ranks under liquid nitrogen cold soaking," *Energy Sources, Part A: Recovery, Utilization, and Environmental Effects*, pp. 1–17, 2020.

[3] D. Qian, L. Xinping, J. Yongsheng, and S. Jinshan, "A numerical simulation of blasting stress wave propagation in a jointed rock mass under initial stresses," *Applied Sciences*, vol. 11, 2021.

[4] X. Sun, G. Chen, J. Li et al., "Propagation characteristics of ultrasonic P-wave velocity in artificial jointed coal briquettes," *Journal of Geophysics and Engineering*, vol. 17, no. 5, pp. 827–837, 2020.

[5] S. Wang, X. Li, and Q. Qin, "Study on surrounding rock control and support stability of ultra-large height mining face," *Energies*, vol. 15, 2022.

[6] Z. Zhang, W. Gao, K. Li, and B. Li, "Numerical simulation of rock mass blasting using particle flow code and particle expansion loading algorithm," *Simulation Modelling Practice and Theory*, vol. 104, article 102119, 2020.

[7] H. Zhou and C. He, "Propagation law of stress wave and cracks in non-penetrating jointed rock mass: a numerical study based on particle flow code," *International Journal*, vol. 38, no. 4, pp. 3967–3981, 2020.

[8] X. Zhou, S. Wang, X. Li et al., "Research on theory and technology of floor heave control in semicoal rock roadway: taking Longhu coal mine in Qitaihe mining area as an example," *Lithosphere*, vol. 2022, Article ID 3810988, 17 pages, 2022.

[9] Y. Li, L. Yashi, Z. Rui, and Z. Jianbo, "Experimental study of blasting wave propagation in jointed rock mass and vibration reduction effect of barrier holes," *IOP Conference Series: Earth and Environmental Science*, vol. 570, no. 4, article 042026, 2020.

[10] S. Zeng, S. Wang, B. Sun, and Q. Liu, "Propagation characteristics of blasting stress waves in layered and jointed rock caverns," *Geotechnical and Geological Engineering*, vol. 36, no. 3, pp. 1559–1573, 2018.

[11] Z. Aliabadian, M. Sharafisafa, A. Mortazavi, and P. Maarefvand, "Wave and fracture propagation in continuum and faulted rock masses: distinct element modeling," *Arabian Journal of Geosciences*, vol. 7, no. 12, pp. 5021–5035, 2014.

[12] A. Sainoki and H. S. Mitri, "Dynamic modelling of fault slip induced by stress waves due to stope production blasts," *Rock Mechanics and Rock Engineering*, vol. 49, no. 1, pp. 165–181, 2016.

[13] G.-a. Zhu, L.-m. Dou, Y. Liu et al., "Dynamic behavior of fault slip induced by stress waves," *Shock and Vibration*, vol. 2016, Article ID 4386836, 13 pages, 2016.

[14] X. Feng, Q. Zhang, E. Wang, M. Ali, Z. Dong, and G. Zhang, "3D modeling of the influence of a splay fault on controlling the propagation of nonlinear stress waves induced by blast loading," *Soil Dynamics and Earthquake Engineering*, vol. 138, p. 106335, 2020.

[15] K. Gao, P. Huang, Z. Liu, J. Liu, C. Shu, and G. Qiao, "Coal-rock damage characteristics caused by blasting within a reverse fault and its resultant effects on coal and gas outburst," *Scientific Reports*, vol. 11, no. 1, p. 19158, 2021.

[16] K. Gao, Z. Liu, J. Liu, F. Zhu, G. Qiao, and S. Zhang, "Application research of directional cumulative blasting for weakening reverse faults in fully mechanized excavation face," *Chinese Journal of Rock Mechanics and Engineering*, vol. 38, pp. 1408–1419, 2019.

[17] G. Wang, X. Wang, and S. Hu, "A dynamic measurement method of elastic modulus of weak interlayer of rock mass," *Chinese Journal of Rock Mechanics and Engineering*, vol. 34, pp. 1828–1835, 2015.

[18] C. Liu, J. Zhang, and P. Cui, "Energy evolution and stress response during stress wave prorogation in the intercalation," *Rock and Soil Mechanics*, vol. 39, pp. 2267–2277, 2018.

[19] N. Sun, M. Lei, Y. Zhang, G. Su, and G. Huang, "A study on the influence of weak interlayer on the propagation process of explosion stress wave," *Journal of Vibration and Shock*, vol. 39, pp. 112–119, 2020.

[20] L. Chen, S. Fan, C. Zhao, L. Zhang, and Z. Cheng, "Calculation method of overburden damage height based on fracture mechanics analysis of soft and hard rock Layers," *Geofluids*, vol. 2019, Article ID 3790264, 15 pages, 2019.

[21] M. Dong, L. Wang, B. Shahbodagh, X. Du, S. Deng, and Z. Sun, "Effect of the soft and hard interbedded layers of bedrock on the mechanical characteristics of stabilizing piles," *Applied Sciences*, vol. 10, no. 14, p. 4760, 2020.

[22] L. Ning, M. Zhanguo, G. Peng, Q. Fuzhou, W. Tuo, and C. Shixing, "Simulation research on the load transfer mechanism of anchoring system in soft and hard composite rock strata under tensile loading conditions," *Advances in Materials Science and Engineering*, vol. 2020, Article ID 9097426, 20 pages, 2020.

[23] X. Sun, G. Li, C. Zhao, Y. Liu, and C. Miao, "Investigation of deep mine shaft stability in alternating hard and soft rock strata using three-dimensional numerical modeling," *Processes*, vol. 7, 2018.

[24] Y. Wang, Y. Zhang, Z. Zhu, M. Du, and Y. Qi, "A novel method for analyzing the factors influencing ground settlement during shield tunnel construction in upper-soft and lower-hard fissured rock strata considering the coupled hydro-mechanical properties," *Geofluids*, vol. 2020, Article ID 6691157, 13 pages, 2020.

[25] C. Shi, D.-j. Li, K.-h. Chen, and J.-w. Zhou, "Failure mechanism and stability analysis of the Zhenggang landslide in Yunnan Province of China using 3D particle flow code simulation," *Journal of Mountain Science*, vol. 13, no. 5, pp. 891–905, 2016.

[26] P. Wang, F. Ren, and M. Cai, "Influence of joint geometry and roughness on the multiscale shear behaviour of fractured rock mass using particle flow code," *Arabian Journal of Geosciences*, vol. 13, no. 4, p. 165, 2020.

[27] X.-x. Yang, H.-w. Jing, K.-f. Chen, and S.-q. Yang, "Failure behavior around a circular opening in a rock mass with non-persistent joints: a parallel-bond stress corrosion approach," *Journal of Central South University*, vol. 24, no. 10, pp. 2406–2420, 2017.

[28] P. A. Cundall and O. D. L. Strack, "A discrete numerical model for granular assemblies," *Géotechnique*, vol. 29, no. 1, pp. 47–65, 1979.

[29] D. O. Potyondy and P. A. Cundall, "A bonded-particle model for rock," *International Journal of Rock Mechanics and Mining Sciences*, vol. 41, no. 8, pp. 1329–1364, 2004.

[30] N. Cho, C. D. Martin, and D. C. Sego, "A clumped particle model for rock," *International Journal of Rock Mechanics and Mining Sciences*, vol. 44, no. 7, pp. 997–1010, 2007.

[31] W. Yuan, W. Wang, X. Su et al., "Numerical study of the impact mechanism of decoupling charge on blasting-enhanced permeability in low-permeability sandstones," *International Journal of Rock Mechanics and Mining Sciences*, vol. 106, pp. 300–310, 2018.

[32] S. Chong, Z. Qiang, and W. Sheng-nian, "Numerical simulation technology and application with particle flow code(PFC5.0)," *Rock and Soil Mechanics*, vol. 39, p. 36, 2018.

[33] G. Wenle, Z. Zehua, L. Baojie, L. Kunpeng, and L. Zhixiong, "Study on numerical simulation of geometric elements of blasting funnel based on PFC5.0," *Shock and Vibration*, vol. 2021, Article ID 8812964, 13 pages, 2021.

[34] G. Kouroussis, O. Verlinden, and C. Conti, "Finite-dynamic model for infinite media: corrected solution of viscous boundary efficiency," *Journal of Engineering Mechanics*, vol. 137, no. 7, pp. 509–511, 2011.

[35] J. Cui, L. Xie, W. Qiao, L. Qiu, Z. Hu, and L. Wu, "Study on blasting characteristics of rock mass with weak interlayer based on energy field," *Scientific Reports*, vol. 12, no. 1, p. 12698, 2022.

[36] L. Xie, Q. Zhu, Y. Qin, J. Wang, and J. Qian, "Study on evolutionary characteristics of toppling deformation of anti-dip bank slope based on energy field," *Sustainability*, vol. 12, no. 18, p. 7544, 2020.

[37] D.-Y. Guo, H.-J. Zhang, P.-F. Lu, and G.-W. Zhang, "Effect of fault on deep-hole cumulative blasting to improve coal bed permeability," *Beijing Keji Daxue Xuebao/Journal of University of Science and Technology Beijing*, vol. 36, pp. 1281–1286, 2014.